Acousto-Optical Volumetric Sensing of Acoustic Fields

Samuel A. Verburg[*] and Efren Fernandez-Grande[†]

Acoustic Technology, Department of Electrical Engineering, Technical University of Denmark, Ørsteds Plads B. 352, Kongens Lyngby DK-2800, Denmark

The characterization of sound fields over space is fundamental in acoustics. Yet, the volumetric acquisition of sound fields using conventional electromechanical transducers is challenging due to the high sampling requirements needed in a three-dimensional domain. In this study, we introduce an acousto-optic sensing method to remotely sample acoustic fields in a volume using a sparse set of noninvasive optical measurements. Optical methods that use light as a sensing element have drawn significant attention recently, since they allow for remote, noninvasive sampling of acoustic fields with fine spatial resolution. The practical deployment of optical sensing in acoustics, however, has been hindered by the limited acquisition of data available, and the unsuitability of existing methods to reconstruct sound fields in scarce-data regimes. The proposed methodology relies on projecting the measured data on a basis that satisfies the wave equation, thus alleviating the measurement requirements associated with traditional reconstruction methods. The proposed approach leads to accuracy improvements of 20 dB relative to current methods, and a 90% reduction of measured data. We demonstrate the approach experimentally by reconstructing *in situ* the three-dimensional sound field inside a room from remote measurements of the acousto-optic interaction. These results are key to advancing the use of acousto-optical sensing methods, which are currently limited to simplified domains. The work presented in this paper brings about the possibility to solve so far intractable problems, such as the volumetric and remote acquisition of complex three-dimensional acoustic fields.

I. INTRODUCTION

The observation and measurement of audible sound generally involves the immersion of electromechanical transducers into a sound field, in order to sense fluctuations of the pressure about its static value. Since the advent of acoustic transduction, acoustic sensing has predominantly consisted of recording pressure variations at a single point in space. The use of arrays of transducers was a definite breakthrough, enabling to capture spatial properties of sound fields, and observe important acoustic propagation phenomena [1,2]. Yet the wide-band acquisition of an arbitrary acoustic field over space is still intractable, as wavelengths of audible sound comprise orders of magnitude ranging from 17 m to 17 mm—resulting in unfeasible sampling requirements.

From the perspective of acoustic sensing, the acousto-optic interaction principle is a promising paradigm, as it enables the sensing of sound over space remotely, with fine spatial resolution, and without immersing transducers into the sound field. The acousto-optic interaction describes the diffraction, deflection, and retardation effects that light

experiences as it traverses acoustic fields in transparent media. Since it was predicted in 1922 [3] and experimentally observed in 1932 [4,5], the diffraction of light due to pressure waves has been exploited to develop light modulators and deflectors [6,7], to study the composition of gases [8], and to characterize pressure waves [9–11].

Acousto-optic sensing methods use light as a sensing element, measuring the effects that pressure waves induce on a light beam in order to probe the acoustic field. Several acousto-optic sensing methods exist that are based on the diffraction and deflection of light [9,11–13]. Measurements of the change in the phase of light induced by acoustic waves, as originally proposed by Jia *et al.* [14], are of particular interest to this study. Unlike measurements with conventional electromechanical transducers, acousto-optic methods do not provide the acoustic pressure at specific locations, since the acousto-optic interaction occurs along the entire optical path. Tomographic techniques, as commonly seen in medical imaging [15,16] or nondestructive testing [17,18], make it possible to reconstruct an image from its projection measurements, and have recently been used to reconstruct two-dimensional (2D) axisymmetrical sound fields in the audible frequency range [19,20].

Yet conventional tomographic techniques are ill suited for observing acoustic fields: classical algorithms require

---

*saveri@elektro.dtu.dk
†efg@elektro.dtu.dk

that the object is scanned uniformly along parallel or fan-shaped beams at regular rotation intervals, and incomplete data result in large reconstruction artifacts. These restricting measurement configurations and high sampling requirements have hindered the development of acousto-optic tomography to measure and visualize audible sound fields, currently limited to simplified domains, such as 2D axisymmetrical sound fields.

In this study we introduce a tomographic method to reconstruct three-dimensional wave fields, and examine the acousto-optic reconstruction problem. The methodology consists in projecting the measured data on a basis that satisfies the wave equation, alleviating the measurement requirements associated with traditional reconstruction methods, and making it possible to observe arbitrary acoustic fields in a volume from a sparse set of optical measurements—remotely and noninvasively. The developments presented in this study constitute a substantial advance in the way we measure and analyze acoustic data, enabling a wide-band capture of spatiotemporal sound fields over extended regions of space. Ultimately, the methodology is of value in other disciplines concerned with the measurement and visualization of wave fields.

II. SENSING PRINCIPLE

The physical principle behind phase-shift acousto-optic sensing is outlined in the following section. The phase shift experienced by a laser beam traversing the harmonic pressure field $p(\mathbf{r})e^{i\omega t}$ is

$$\delta\phi = \frac{2\pi}{\lambda_\ell}\frac{\partial n}{\partial p}i\omega\int_L p(\mathbf{r})dl, \tag{1}$$

which shows that the measured phase shifts are proportional to the projection of the pressure field along the light beam $\int_L p(\mathbf{r})dl$. In Eq. (1), $\mathbf{r}$ is the position vector, l is an integration variable along the path followed by the beam, L is the length of the path, λ_ℓ is the optical wavelength, and ω is the acoustic frequency. The temporal dependency $e^{i\omega t}$ is omitted for convenience. The piezo-optic coefficient $\partial n/\partial p$ is characteristic of the medium, here assumed homogeneous and isotropic. A linear relation between the index of refraction n and the acoustic pressure p [implicit in Eq. (1)] can be derived for several media, including air [19]. An optical interferometer capable of measuring the acoustically induced phase shifts of light is shown in Fig. 1(a). It is assumed that the surface on which the laser beam is backscattered, $\partial\Omega$, is fixed, i.e., the phase shift induced by its vibration is much smaller than the phase shift due to the acousto-optic interaction. Otherwise, an additional term has to be included in Eq. (1) to account for the surface vibration velocity (further details are given in the Supplemental Material [21]).

III. RECONSTRUCTION METHODS

A brief theoretical background on classical tomography along with the proposed reconstruction method are described in this section.

A. Classical tomography

The most common tomographic reconstruction technique is the *filtered backprojection* (FBP), which is based on the Radon transform

$$S(x',\theta) = \int_{-\infty}^{\infty} p(x,y)dy', \tag{2}$$

where (x',y') is the rotated coordinate system [see Fig. 1(b)]. The estimation of the pressure field is computed
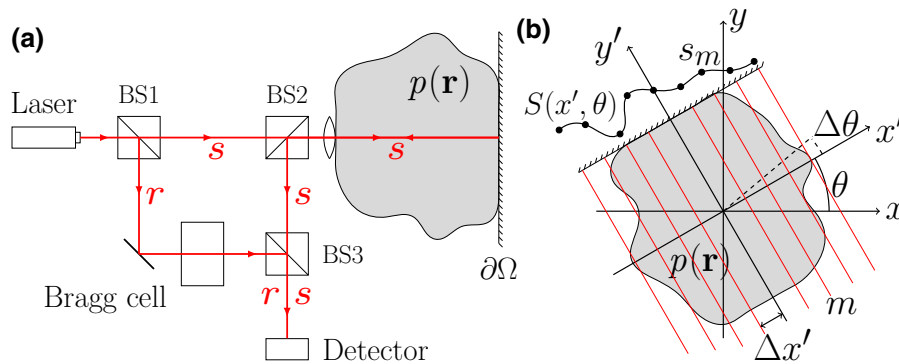

FIG. 1. (a) Optical interferometer used to measure acoustically induced phase shifts of light. A laser beam is generated and split into a sensing branch s and a reference branch r. The sensing beam is sent through the sound field $p(\mathbf{r})$, where it is backscattered off the surface $\partial\Omega$, and collected back at BS2. After passing through BS3, both branches interfere on a photodiode detector, which generates an electrical current proportional to the acoustically induced phase shift of the sensing beam. (b) Tomographic scan of $p(\mathbf{r})$ with parallel beams. The projections $S(x',\theta)$ are sampled with beams of equal spacing $\Delta x'$ and rotation increment $\Delta\theta$. A sample of the projection measured by a single beam m is s_m.

as $p(x,y) = \int_0^\pi Q(x', \theta)d\theta$, where Q is the projection S filtered in the Fourier domain [22]. It is important to note that transform-based approaches (such as FBP) require that the test object is scanned uniformly, with sufficient resolution, from every direction, and that the scan lines are either parallel or fan shaped.

In cases where it is not possible to uniformly scan the object, *algebraic reconstruction techniques* (ARTs) are used [22], where the problem is formulated as a linear system of unknowns and equations. The projection s_m sensed by a single beam m can be written as

$$s_m = \int p(\mathbf{r})dl_m \approx \sum_{n=1}^N a_n \int b_n(\mathbf{r})dl_m, \quad (3)$$

where l_m is the path followed by the beam. The object is approximated with a set of N basis functions $\{b_1, \ldots, b_N\}$ and their corresponding expansion coefficients $a_1, \ldots, a_N$, such that $p \approx \sum_{n=1}^N a_n b_n$. ART methods discretize the reconstructed object into N pixels with a constant value of p. Algebraic approaches overcome the uniform-sampling limitation associated with transform-based algorithms [Eq. (2)] because arbitrary rays can be included in the system of equations. However, ART methods require an unfeasibly large number of measurements, as finite pixels constitute a suboptimal basis when the goal is to represent a wave field.

B. Proposed wave-expansion reconstruction

The measurement requirements of classical tomography methods are highly limiting: the ART inefficient pixel-based representation and the FBP uniform sampling limit their potential as reconstruction approaches for observing sound fields via acousto-optic sensing. In this study, we propose the use of reconstruction bases that satisfy the wave equation. We introduce elementary plane waves to expand the pressure field; thus, the projection s_m becomes

$$s_m = \int p(\mathbf{r})dl_m \approx \sum_{n=1}^N a_n \int e^{i\mathbf{k}_n \cdot \mathbf{r}}dl_m, \quad (4)$$

where $\mathbf{k}_n$, defined as the wave number vector, indicates the direction of propagation of the nth wave in the expansion. If only propagating plane waves are included, the length of the wave number vectors is $|\mathbf{k}| = \omega/c$, where c is the speed of sound in the medium [23]. The order of discretization of the radiation sphere is N, and the convergence of this approximation is theoretically guaranteed [24–27]. Equation (4) can be written algebraically as

$$\mathbf{s} \approx \mathbf{Ha}, \quad (5)$$

where $\mathbf{s} \in \mathbb{C}^M$ is a vector that contains M measured projections, $\mathbf{a} \in \mathbb{C}^N$ corresponds to the unknown coefficients of the N plane waves in the expansion, and $\mathbf{H} \in \mathbb{C}^{M \times N}$ is a matrix with elements $h_{m,n} = \int e^{i\mathbf{k}_n \cdot \mathbf{r}}dl_m$. The estimation of the wave number function on the radiation sphere from pressure measurements constitutes a classical ill-posed problem. Consequently, regularization is necessary to determine a stable solution for the expansion coefficients a_n [28,29]. The regularized problem is defined as

$$\tilde{\mathbf{a}} = \arg \min_{\mathbf{a} \in \mathbb{C}^N} ||\mathbf{a}||_2 \quad \text{subject to} \quad ||\mathbf{s} - \mathbf{Ha}||_2 \le \epsilon, \quad (6)$$

where $||\mathbf{a}||_2 = (\sum_i |a_i|^2)^{1/2}$, and ϵ is the size of the discrepancy permitted between the measurements $\mathbf{s}$ and the representation $\mathbf{Ha}$. Once the wave coefficients are estimated, the reconstructed sound field is calculated as

$$\tilde{\mathbf{p}} = \mathbf{G}\tilde{\mathbf{a}}, \quad (7)$$

where $\tilde{\mathbf{p}} \in \mathbb{C}^L$ contains the pressure estimated at positions $\mathbf{r}_1, \ldots, \mathbf{r}_L$, and $\mathbf{G} \in \mathbb{C}^{L \times N}$ is a matrix with elements $g_{l,n} = e^{i\mathbf{k}_n \cdot \mathbf{r}_l}$.
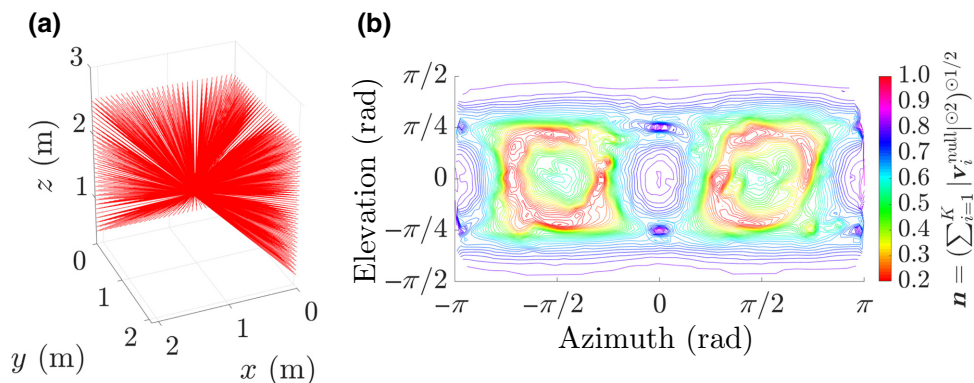

FIG. 2. (a) Sampling scheme with $M = 1682$ measurements distributed inside two square-pyramidal volumes of base 2.1×2.1 m^2 and height 1.15 m. (b) Vector $\mathbf{n} = (\sum_{i=1}^K |\mathbf{v}_i^{\text{null}}|^{\odot 2})^{\odot 1/2}$ for the null-space orthonormal basis of the measurement set shown in (a). The x and y axes represent the azimuth and elevation angles of the wave coefficients over the radiation sphere. The number of waves included in the expansion is $N = 2500$, and the acoustic frequency is set to 3000 Hz.

C. Null-space analysis

The spatial integration involved in the acousto-optic interaction, i.e., Eq. (1), can lead to zero-valued samples—e.g., if p is composed of a single wave propagating with direction ψ, the integral of Eq. (1) for a beam of orientation ψ and length L is zero for acoustic wavelengths $\lambda = L/n$ with $n = 1, 2, \ldots$. Therefore, care must be taken to select a suitable set of measurements to ensure that the sampling is complete. In this study we verify the validity of the sensing method via a null-space analysis, which indicates the sufficient conditions to represent the solution of a linear system and thus reconstruct a signal correctly.

While classical tomographic sampling, using rotational uniform projections, can be related to pointwise sampling through the projection-slice theorem [22], such closed-form relations are not defined for asymmetric, nonuniform projections. Yet the validity of any sampling method can be assessed by studying the null space of its sensing matrix [30]: waves whose direction coincide with the sensing beam orientation integrate to zero [see Eq. (1)], and therefore the corresponding coefficients lie in the null space of **H**. This loss of sensitivity to certain directions is common to all tomographic reconstruction methods when sensing wave fields. The null space of **H** is defined as $\mathcal{N}(\mathbf{H}) := \{\mathbf{a} \in \mathbb{C}^N | \mathbf{Ha} = \mathbf{0}\}$, i.e., a vector in the null space of **H** is mapped to the zero vector. Note that $\mathcal{N}(\mathbf{H})$ depends only on the sampling beams, and not on the specific sound field to be reconstructed. The null space can be computed via the singular value decomposition, $\mathbf{H} = \mathbf{U}\boldsymbol{\Sigma}\mathbf{V}^H$, where $\mathbf{U} \in \mathbb{C}^{M \times M}$ and $\mathbf{V} \in \mathbb{C}^{N \times N}$ are unitary matrices, and $\boldsymbol{\Sigma} \in \mathbb{R}^{M \times N}$ is a diagonal matrix with non-negative, nonincreasing entries, known as the singular values. An orthonormal basis for $\mathcal{N}(\mathbf{H})$ is formed by the K columns of **V** that do not correspond to nonzero singular values, $\mathbf{v}_1^{\text{null}}, \ldots, \mathbf{v}_K^{\text{null}}$. The validity of the measurement set can then be determined by the vector $\mathbf{n} = (\sum_{i=1}^{K} |\mathbf{v}_i^{\text{null}}|^{\odot 2})^{\odot 1/2}$, where each element n_j ranges from zero (when the jth wave component lies fully in the column space of **H**) to one (when the jth wave component lies fully in the null space of **H**).

Figure 2(a) shows a set of optical measurements for sampling a three-dimensional domain. Figure 2(b) shows the corresponding null-space orthonormal basis vector **n**, indicating that sampling is complete, as none of the elements of **n** reach one—i.e., no wave coefficient is fully contained in the null space of the sensing matrix. As the sampling contains beams approximately perpendicular to each wave direction, none of the wave components integrate to zero for all beams, making it possible to resolve waves propagating in any direction. The results of this analysis demonstrate the validity of the reconstruction method.
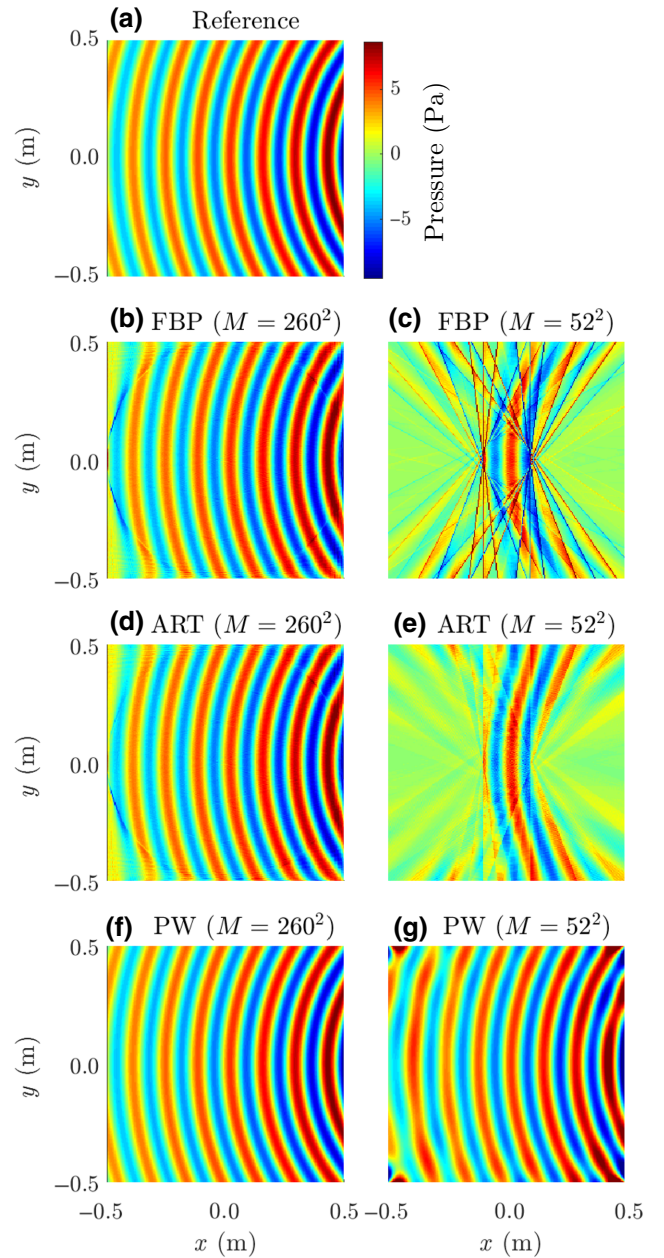

FIG. 3. Comparison of the proposed wave-based reconstruction method with traditional tomographic FBP and ART algorithms. (a) Reference sound field (real part), generated by a monopole radiating in free field with a frequency of 2.5 kHz on a 1×1 m^2 plane. The pressure is calculated at $N = 260^2$ points on the plane. Projections are sampled along $M_{x'}$ parallel beams (uniformly spaced by $1/\sqrt{N}$ m) at M_θ uniform rotation angles, resulting in a total of $M = M_{x'} \times M_\theta$ measurements [see Fig. 1(b)]. (b)–(e) Reconstructions achieved by the FBP and ART algorithms, using $M = 260^2$ and $M = 52^2$ measurements, respectively (reconstructions computed with the ASTRA toolbox [31]). (f),(g) Reconstructions achieved by the proposed method (PW), based on a plane-wave expansion of the sound field, using $M = 260^2$ and $M = 52^2$ measurements, respectively.
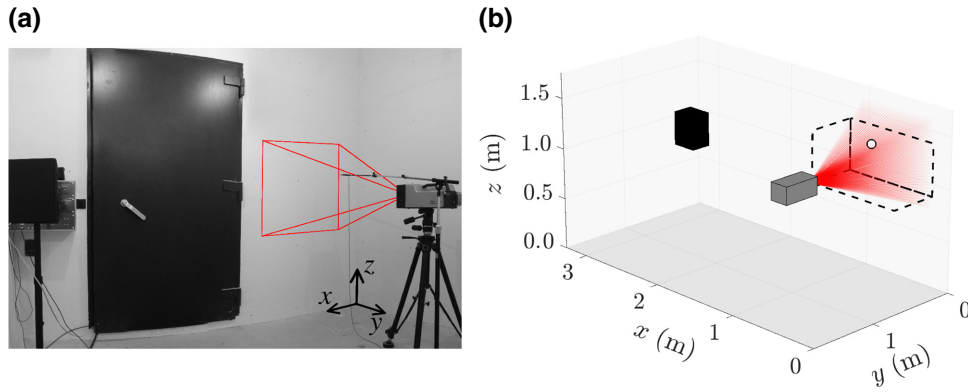
FIG. 4.   Experimental setup. (a) Picture of the room, interferometer, and loudspeaker. The room has dimensions $3.29 \times 4.38 \times 3.28$ m^3. The room walls, floor, and ceiling are made of concrete, and no special retroreflecting covering is applied to the surfaces (just regular white paint). Two of the walls (the y-z wall closer to the loudspeaker and the x-z wall opposite to the scanned surface) are treated with acoustically absorptive material, which attenuates the reflections from such surfaces. The average reverberation time of the room in the studied frequency range (1 to 4 kHz) is 1.1 s. (b) Schematic of the measurement setup. The sound field is generated by a loudspeaker (in black) placed sideways with respect to the interferometer (in gray). The sound field is sampled with $M = 814$ beams (in red), and reconstructed in a rectangular volume (dashed line). A null-space analysis of this sampling scheme is included in the Appendix.

IV. EXPERIMENTAL RESULTS

A. Numerical study

A comparison between traditional reconstruction approaches and the proposed method is shown in Fig. 3 using noiseless synthetic data (noisy reconstructions are shown in Ref. [21] for completeness, which lead to similar conclusions). The sound field generated by a point source is calculated on a plane [see Fig. 3(a)], and uniformly sampled along M beams. Two sampling conditions are studied: one in which the projections are measured over the entire plane (where the number of measured projections is $M = 260^2$), and one decimated configuration where projections are measured only in the center of the plane ($M = 52^2$). Two measures are used to assess the accuracy of the reconstructions: the normalized mean squared error in decibels, $\text{NMSE}_{\text{dB}} = 20 \log_{10}(||\mathbf{p} - \tilde{\mathbf{p}}||_2/||\mathbf{p}||_2)$, and the normalized correlation $C_\% = 100|\mathbf{p} \cdot \tilde{\mathbf{p}}|/(||\mathbf{p}||_2||\tilde{\mathbf{p}}||_2)$, where $\mathbf{p}$ is the reference pressure [Fig. 3(a)] and $\tilde{\mathbf{p}}$ is the estimated one (by either FBP, ART, or the proposed method, denoted PW). Throughout this study the 2-norm is chosen as the regularization term and the L-curve method, as implemented in Ref. [32], is used to find the regularization parameter. See the details on regularization in the Supplemental Material [21]. The FBP and ART reconstructions are shown in Figs. 3(b) to 3(e), respectively. When the entire plane is measured [$M = 260^2$; Figs. 3(b) and 3(d)], accurate reconstructions are achieved by both FBP and ART algorithms, with only noticeable errors at the corners of the aperture. The complete sampling condition results in a low normalized mean squared error (-16.7 dB for FBP and -17.8 dB for ART), and a high correlation

(98.9% for FBP and 99.2% for ART). However, the reconstruction degrades drastically when the number of projections is decimated to $M = 52^2$ [Figs. 3(c) and 3(e)]. In this case, the sound field is correctly recovered only in approximately $\frac{1}{25}$th of the total area, corresponding to the central region (the only area with a sufficient sampling density). The decimated number of projections leads to a high normalized mean squared error (-0.2 dB for FBP and -1.4 dB for ART), and a reduced correlation (38.3% for FBP and 52.3% for ART). Conversely, the proposed methodology [based on Eq. (4)] yields correct reconstructions for both the complete [Fig. 3(f), with a normalized mean squared error of -41.7 dB and a correlation of 100%] and decimated [Fig. 3(g), with a normalized mean squared error of -12.7 dB and a correlation of 97.5%] sampling, only exhibiting some deviations on the edges of the domain when the projections are decimated to $M = 52^2$ projections. These results indicate an improvement in accuracy of 20 dB and a reduction of 90% of measured projections with respect to FBP and ART. The correlation results between the reconstructions and the true field are shown in Table I.

TABLE I.   Normalized correlation between the reference (true field) and reconstructed sound fields of Fig. 3.

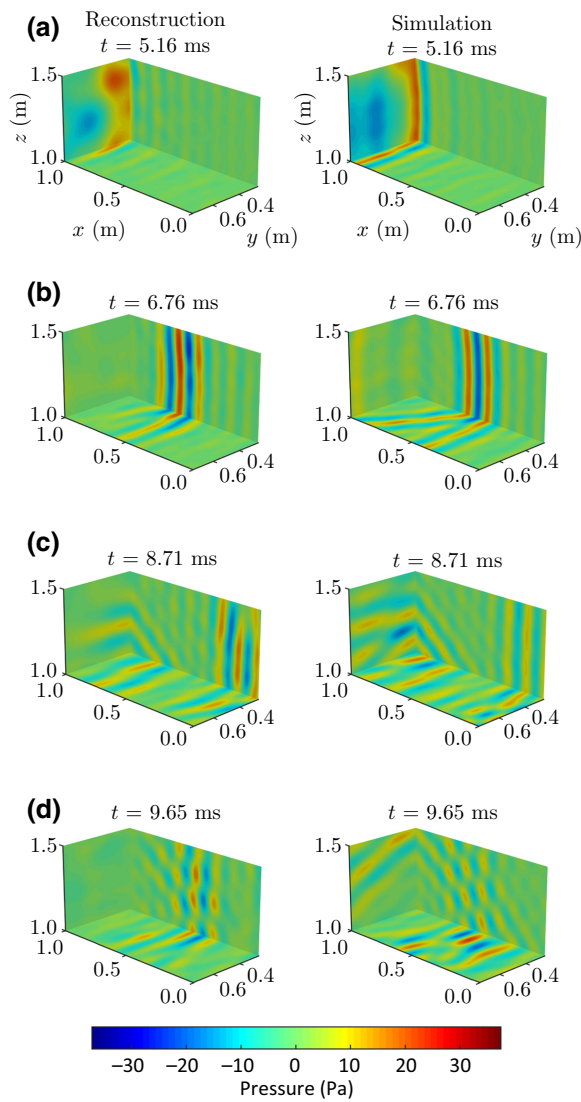| Number of projections M	Normalized correlation		
	FBP (%)	ART (%)	PW (%)
260^2	98.9	99.2	100
52^2	38.3	52.3	97.5

FIG. 5. Time-domain sound field in a room at four time frames: (a) 5.16 ms, (b) 6.76 ms, (c) 8.71 ms, and (d) 9.65 ms. The colored surfaces represent the pressure on three of the faces of the rectangular volume in which the sound field is reconstructed. The sound field is band limited between 1.5 and 3 kHz. Left column: reconstruction from $M = 814$ optical measurements (see Fig. 4). Right column: numerical simulation of the sound field. The simulation is based on the image source method [33], computed using the implementation in Ref. [34].

B. Characterization of a volumetric sound field

In what follows, we demonstrate experimentally that the proposed method enables us to acquire *in situ* the acoustic field in a room [the experimental setup is shown in Fig. 4(a)]. The acoustically induced phase shifts are measured by directing the beam of a scanning laser Doppler vibrometer (LDV) towards a rigid surface, i.e., one of the room walls. To ensure that the measured phase shifts are due to the acousto-optic interaction, the vibration

velocity of the wall is monitored with an electromechanical accelerometer (results included in the Supplemental Material [21]). Measurements with scanning LDVs are sequential, i.e., the laser beam is sequentially steered in M individual directions, with individual loudspeaker emissions for each direction. The measurement procedure is however automatized once the directions are defined. The number of sampled directions is $M = 814$, with an total acquisition time of approximately 2.9 h. The acoustic field inside the room is sampled automatically with the scanning LDV, and reconstructed within a rectangular volume [see Fig. 4(b)].

The time-domain reconstruction of the sound field in the volume is shown in Fig. 5. The field is displayed on three of the volume faces and at four separate time instances (5.16, 6.76, 8.71, and 9.65 ms). The left column corresponds to the reconstructed sound field, while the right column shows an image source method (ISM) simulation [33] of the acoustic field in the room. The sound arriving from the source can be seen in the *y-z* plane in the first time frame, at $t = 5.16$ ms [Fig. 5(a)]. The front is traveling along the *x* direction in the second frame, at $t = 6.76$ ms [Fig. 5(b)], closely followed by the reflected sound from the wall opposite to the laser. In the third frame, at $t = 8.71$ ms [Fig. 5(c)], the sound radiated from the source is reflected off the wall in front of the source. A reflection from the floor, traveling with a direction oblique to the *x-z* plane, can also be observed. The fourth frame, at $t = 9.65$ ms [Fig. 5(d)], shows the interference pattern resulting from the interaction of the reflections from the wall (in the *x* direction) and from the floor (in the *x, z* oblique direction). A video of the time domain reconstruction and simulation is included in the Supplemental Material [21]. The agreement between reconstruction and numerical simulation is remarkable, even though the simplifying assumptions of the simulation (i.e., monopolar source and specular reflections) do not reproduce some of the phenomena observed experimentally, such as wall scattering and source directivity.

A quantitative assessment of the reconstruction and simulation shown in Fig. 5 is performed. Measurements of the acoustic pressure at 27 positions inside the reconstructed volume are acquired with a high-precision 1/2 in. condenser measurement microphone. The NMSE and correlation are calculated using the first 50 ms of the time-domain pressure measured with the microphone as the reference **p**, and the time-domain reconstructions and simulation as the estimation **p̃**. Figure 6 summarizes the NMSE and correlation results for the 27 positions. The reconstruction achieves a negative NMSE, and a correlation above 40% for most of the 27 positions. On the other hand, the simulation presents higher error (around +2 dB NMSE) and lower correlation (around 20%).

The sound pressure at one specific position (out of the 27) is examined in Fig. 7. The pressure reconstructed
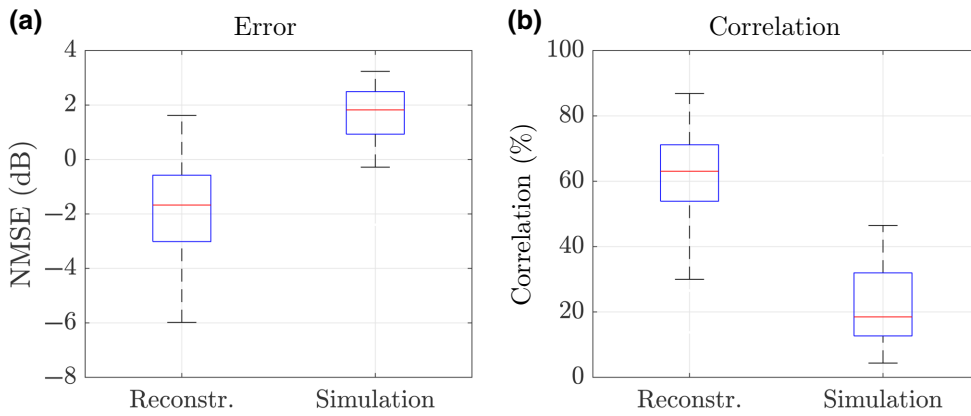
FIG. 6. (a) Normalized mean squared error and (b) normalized correlation achieved by the proposed sensing method and by the simulation for the 27 positions measured with a microphone inside the reconstructed volume. The central red mark indicates the median, the top and bottom of the blue box indicates the 75th and 25th percentiles, and the whiskers extend to the most extreme datapoints not considered outliers.

from optical measurements is compared against the sound pressure measured with the microphone in Fig. 7(a). The numerical simulation of the sound field in the room is also compared to the microphone measurement in Fig. 7(b). The pressure wave radiated from the loudspeaker (at approximately 7 ms) and individual reflections from the room surfaces (at approximately 10, 13, and 16 ms) are recovered by the acousto-optic reconstruction, and align well in time with the reference pressure. On the other hand, the pressure calculated with the numerical simulation is misaligned by approximately 0.25 ms for the reflections at 13 and 16 ms. A quantitative assessment indicates good correlation between reference and reconstruction (84.7%), and a moderate NMSE (-4.58 dB), while for the simulation, both the correlation and NMSE are poor (4.4% and 2.77 dB). This indicates that the deviations found between the simulation and volumetric acousto-optic measurement, shown in Fig. 5, appear to be a result of the simulation model and not of reconstruction error.

It should be noted that the spatiotemporal volumetric reconstruction of the sound field inside a room has this far been an intractable problem. The presented approach constitutes a relevant sensing paradigm to successfully achieve it.

V. CONCLUSION

The proposed acousto-optic tomography method enables us to capture and observe three-dimensional acoustic fields in arbitrary volumes using noninvasive, remote measurements *in situ*. The method formulates an elementary wave expansion of the observed acoustic field, which enables tomographic reconstructions based on a limited set of arbitrary, nonregular field projections. We demonstrate experimentally that the proposed methodology extends the capabilities of acousto-optic sensing of sound fields and enables the volumetric acquisition of audible sound. The method achieves errors 20 dB lower than existing approaches at high sampling rates, or, alternatively, a reduction of measurement projections of approximately 90%. The results presented in this study open a significant experimental approach for problems in acoustics where data
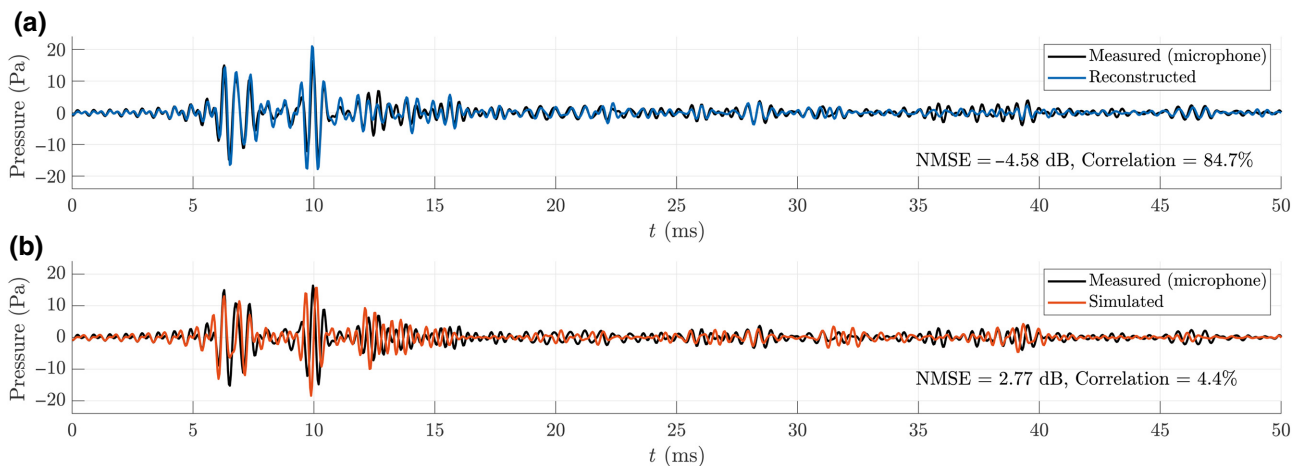

FIG. 7. Acoustic pressure at position $x = 0.572$, $y = 0.378$, $z = 1.370$ inside the sampled volume. Reference pressure measured with a microphone (in black) and (a) reconstructed from optical measurements (in blue) and (b) simulated with the image source method (in red).
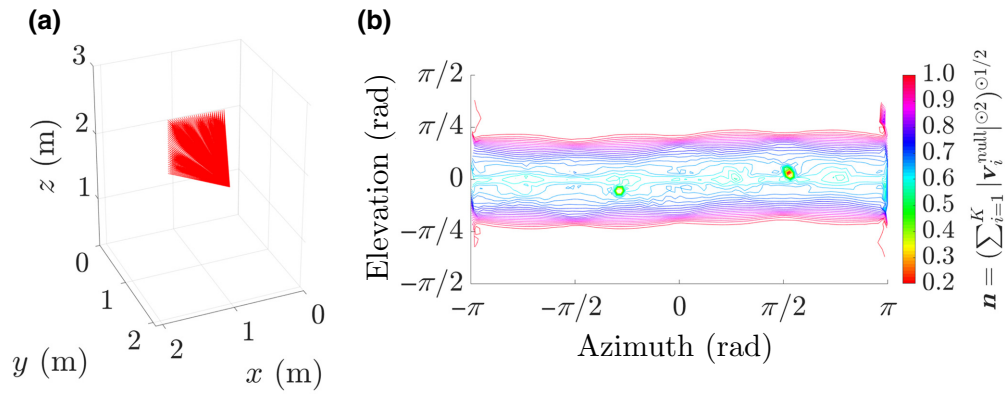
FIG. 8. (a) Sampling scheme with $M = 814$ measurements distributed inside a square-pyramidal volume of base 0.84×0.84 m^2 and height 1.15 m. (b) Vector $\mathbf{n} = (\sum_{i=1}^{K} |\mathbf{v}_i^{\text{null}}|^{\odot 2})^{\odot 1/2}$ for the null-space orthonormal basis of the measurement set shown in (a). The x and y axes represent the azimuth and elevation angles of the wave coefficients over the radiation sphere. The number of waves included in the expansion is $N = 2500$, and the acoustic frequency is set to 3000 Hz.

acquisition is scarce or not accessible (such as, e.g., sound source localization of turbulent flows or the measurement of sound fields inside cavities). Considering its reconstruction accuracy and high acquisition economy, the approach can be of value for other disciplines concerned with the observation of wave fields, and where data availability is limited or incomplete.

ACKNOWLEDGMENTS

APPENDIX: NULL-SPACE ANALYSIS OF THE EXPERIMENTAL SAMPLING SCHEME

Figure 8(a) shows the measurement set used in the experiment inside the room (Fig. 4). Inside the studied room, the x-z wall situated at $y = 4.38$ m is covered with damping material. As a result, waves propagating in the y direction are highly attenuated. Thus, the measurement set does not need to include beams that are perpendicular to the y axis. Figure 8(b) shows the corresponding vector $\mathbf{n}$, which is complete over the hemisphere, indicating that it is suitable for the experiment inside the room—as it can recover the directions where sound waves are present, i.e., in the x and z directions.

[1] E. G. Williams and J. D. Maynard, Holographic Imaging without the Wavelength Resolution Limit, Phys. Rev. Lett. **45**, 554 (1980).

[2] J. D. Maynard, E. G. Williams, and Y. Lee, Nearfield acoustic holography: I. Theory of generalized holography and the development of NAH, J. Acoust. Soc. Am. **78**, 1395 (1985).

[3] L. Brillouin, Diffusion de la lumière et des rayons X par un corps transparent homogène, Ann. Phys. **9**, 88 (1922).

[4] P. Debye and F. W. Sears, On the scattering of light by supersonic waves, Proc. Natl. Acad. Sci. **18**, 409 (1932).

[5] R. Lucas and P. Biquard, Optical properties of solids and liquids under ultrasonic vibrations, J. Phys. Rad. **7**, 464 (1932).

[6] R. Adler, Interaction between light and sound, IEEE Spectr. **4**, 42 (1967).

[7] A. Korpel, *Acousto-Optics* (Marcel Dekker, New York, 1996).

[8] A. C. Tam and W. P. Leung, Optical Generation and Detection of Acoustic Pulse Profiles in Gases for Novel Ultrasonic Absorption Spectroscopy, Phys. Rev. Lett. **56**, 560 (1984).

[9] A. Korpel, Visualization of the cross section of a sound beam by Bragg diffraction of light, Appl. Phys. Lett. **9**, 425 (1966).

[10] W. R. Klein and B. D. Cook, Unified approach to ultrasonic light diffraction, IEEE Trans. Son. Ultrason. **14**, 123 (1967).

[11] R. Reibold and W. Molkenstruck, Light diffraction tomography applied to the investigation of ultrasonic fields. Part I: Continuous waves, Acustica **56**, 180 (1984).

[12] W. Merzkirch, *Flow Visualization* (Academic Press, New York, 1974).

[13] E. Koponen, J. Leskinen, T. Tarvainen, and A. Pulkkinen, Acoustic pressure field estimation methods for synthetic schlieren tomography, J. Acoust. Soc. Am. **145**, 2470 (2019).

[14] X. Jia, C. Matteï, and G. Quentin, Analysis of optical interferometric measurements of guided acoustic waves in transparent solid media, J. Appl. Phys. **77**, 5528 (1995).

[15] A. M. Cormack, Representation of a function by its line integrals, with some radiological applications, J. Appl. Phys. **34**, 2722 (1963).

[16] G. N. Hounsfield, Computerized transverse axial scanning (tomography): Part 1. Description of system, Br. J. Radiol. **46**, 1016 (1973).

[17] B. P. Flannery, H. W. Deckman, W. G. Roberge, and K. L. D'Amico, Three-dimensional X-ray microtomography, Science **237**, 1439 (1987).

[18] P. Cloetens, M. Pateyron-Salomé, J. Y. Buffière, G. Peix, J. Baruchel, F. Peyrin, and M. Schlenker, Observation of microstructure and damage in materials by phase sensitive radiography and tomography, J. Appl. Phys. **81**, 5878 (1997).

[19] A. Torras-Rosell, S. Barrera-Figueroa, and F. Jacobsen, Sound field reconstruction using acousto-optic tomography, J. Acoust. Soc. Am. **131**, 3786 (2012).

[20] K. Yatabe, K. Ishikawa, and Y. Oikawa, Acousto-optic back-projection: Physical-model-based sound field reconstruction from optical projections, J. Sound Vib. **394**, 171 (2017).

[21] See Supplemental Material at http://link.aps.org/supplemental/10.1103/PhysRevApplied.16.044033 for a video of the time domain 3D sound field inside the room, details on the regularization applied, and a study of the influence of noise and vibrations of the reflecting surface.

[22] A. C. Kak and M. Slaney, *Principles of Computerized Tomographic Imaging* (IEEE Press, New York, 1988).

[23] E. G. Williams, *Fourier Acoustics* (Academic Press, San Diego, 1999).

[24] I. N. Vekua, *New Methods for Solving Elliptic Equations* (North-Holland, Amsterdam, 1967).

[25] A. Moiola, R. Hiptmair, and I. Perugia, Plane wave approximation of homogeneous Helmholtz solutions, Z. Angew. Math. Phys. **62**, 809 (2011).

[26] A. Moiola, R. Hiptmair, and I. Perugia, Vekua theory for the Helmholtz operator, Z. Angew. Math. Phys. **62**, 779 (2011).

[27] G. Chardon, A. Cohen, and L. Daudet, Sampling and reconstruction of solutions to the Helmholtz equation, Sampl. Theory Signal Image Process. **13**, 67 (2014).

[28] P. C. Hansen, *Rank-Deficient and Discrete Ill-Posed Problems* (SIAM, Philadelphia, 1998).

[29] R. Kress, *Linear Integral Equations* (Springer-Verlag, New York, 1998), 2nd ed.

[30] K. M. Hanson, in *Image Recovery: Theory and Application* (Academic Press, Orlando, 1987), p. 79.

[31] W. van Aarle, W. J. Palenstijn, J. D. Beenhouwer, T. Altantzis, S. Bals, K. J. Batenburg, and J. Sijbers, The ASTRA toolbox: A platform for advanced algorithm development in electron tomography, Ultramicroscopy **157**, 35 (2015).

[32] P. C. Hansen, Regularization tools: A Matlab package for analysis and solution of discrete ill-posed problems, Numer. Algorithms **6**, 1 (1994).

[33] J. B. Allen and D. A. Berkley, Image method for efficiently simulating small-room acoustics, J. Acoust. Soc. Am. **65**, 943 (1979).

[34] E. A. Habets, Room impulse response generator, Report 2010 (unpublished).